Improved Method for Specifying Solar Wind Speed Near the Sun

Charles N. Arge[*], Dusan Odstrcil[*], Victor J. Pizzo[†], and Leslie R. Mayer[*]

[*]*Cooperative Institute for Research in Environmental Sciences, University of Colorado, Boulder, CO 80309, USA*
[†]*Space Environment Center, National Oceanic and Atmospheric Administration, Boulder, CO 80305, USA*

Abstract. We have found an improved technique for empirically specifying solar wind flow speed near the Sun (~0.1 AU) using a set of three simple inter-linked coronal/solar wind models. In addition to magnetic field expansion factor, solar wind speed also appears to be influenced by the minimum angular distance that an open field footpoint lies from a coronal hole boundary. We conduct our study using polar field corrected Mount Wilson Solar Observatory Carrington maps from 1995. During this period, the Sun was in the declining phase of the solar cycle and the solar wind had relatively simple global structure.

INTRODUCTION

Theoretical understanding of solar wind acceleration remains elusive. To date, the most common methods for predicting solar wind speed near Earth are based on empirical methods or interplanetary scintillation (IPS) techniques [1]. The focus of this paper is on the first approach.

In 1990, Wang and Sheeley (WS) [2] found a correlation between solar wind speed at L1 and magnetic field expansion factor (f_s) of open coronal field lines, where f_s is defined as the rate that a flux tube expands (compared to purely radial expansion) from 1 $R_\odot$ to a "source surface" positioned ~2-3 $R_\odot$ from Sun center. WS used a potential field source surface (PFSS) model [3,4,5] to identify open field lines and to calculate their expansion factors. Arge et al. [6] have recently applied a modification of the WS method for space weather forecasting purposes and now routinely predict solar wind speed and interplanetary field polarity (IMF) polarity at Earth (http://www.sec.noaa.gov/ws/). The modification consists of deriving an empirical relationship between f_s and solar wind speed (v_{sw}) at 2.5 $R_\odot$ (i.e., at the source surface) rather than at L1. This empirical function was found by iteratively testing various mathematical relationships between f_s and v_{sw}, using it to assign the solar wind speed at the source surface, propagating the wind out to L1, and then comparing the results with observations. The procedure was repeated until a best fit was found. A simple 1-D modified kinematic (1-DMK) model, which included an ad hoc method to account for stream interactions, was used to transport the wind to L1.

We report here on our effort to find an improved empirical relationship between solar wind speed near the Sun (~0.1 AU) and various photospheric and coronal field parameters. We have found a new relationship for specifying solar wind speed, which is a function of both f_s and the minimum angular separation (at the photosphere) between an open field footpoint and its nearest coronal hole boundary (θ_b). The new relationship works much better than one derived previously, which is a function of f_s only. We focus here on the solar wind during 1995, as we have had past difficulty successfully predicting the stream structure for this period.

APPROACH

Solar wind observations made at L1 must be mapped back to the Sun to compare with photospheric and coronal field parameters. We mapped WIND spacecraft observations from 1995 back to 0.1 AU (i.e., 21.5 $R_\odot$) assuming constant flow speed, neglecting stream interactions, but accounting for solar rotation. While simple, this approach has been shown to work reasonably well [7]. To relate the mapped-back solar wind with observed photospheric and derived coronal field parameters, a PFSS model (representing the field configuration of the inner corona from 1 to 2.5 $R_\odot$) was used in combination with the Schatten current sheet (SCS) model [8] (representing the field configuration of the outer corona between 2.5 and 21.5 $R_\odot$). Together, these models permit open field lines to be identified and then traced down to the photosphere. Daily updated photospheric field maps from Mount Wilson Solar Observatory (MWO) (grid resolution 5°×5°) were used as input to the models. The PFSS+SCS model combination was run for each daily updated map available from 1995.

Field lines located on the outer boundary of the SCS model and positioned at the appropriate sub-earth point for a given date and time are the relevant ones for this study. The (mapped-back) solar wind speeds associated

CP679, *Solar Wind Ten: Proceedings of the Tenth International Solar Wind Conference*,
edited by M. Velli, R. Bruno, and F. Malara

with these particular field lines are compared with the following five photospheric and coronal parameters: expansion factor (f_s) evaluated at 2.5 $R_\odot$, photospheric (or footpoint) field strength (B_{ph}), and the minimum (spherical) angular separation between an open field footpoint and 1) sub-earth point (θ_{se}), 2) current sheet (θ_{cs}), and 3) nearest coronal hole boundary (θ_b). These parameters are plotted in Figure 1 in five separate panels with solar wind speed at 21.5 $R_\odot$ over-plotted in each.

Interpreting the results in Figure 1 is complicated. For instance, the procedure used to map the solar wind from L1 back to 21.5 $R_\odot$ is, without doubt, overly simple and certainly can result in large errors, potentially masking statistical correlations between the parameters and v_{sw}. Yet, it is surprising how clear the inverse correlation between f_s and v_{sw} appears in the top panel of Figure 1. In fact, we obtained a correlation coefficient of –0.55 between these two quantities, which is very similar to the one found originally by WS. Nevertheless, one can see that a given expansion factor does not necessarily correspond to the same solar wind speed. For instance, note the values of f_s and v_{sw} for the high-speed stream located between Carrington rotations (CR) 1893 and 1894 (i.e., Panel 1 of Figure 1), and compare the same quantities for the stream located just after the start of CR 1900. This clearly suggests that solar wind speed is a function of more than just f_s.

Because of all the uncertainties with the mapped-back solar wind and the possibility that v_{sw} is a complicated function of the above-mentioned parameters, we take the following approach. First, search for patterns between solar wind speed and the above five photospheric/coronal parameters. Second, deduce an empirical relationship for v_{sw} involving one or more these parameters. Third, assign v_{sw} at the outer boundary of the SCS model, and then, for each daily updated map from 1995, propagate the solar wind out to Earth using a 1-D modified kinematic (1-DMK) code. Fourth, directly compare predictions with observations. For this particular study, the 1-DMK code is preferred over a more advanced 3-D MHD code, as it significantly reduces the time required for each new trial run.

While tedious, the main advantage of the approach just described is that it relies only on the mapped-back solar wind for deducing the empirical velocity function. Propagating the solar wind from the Sun to L1 using our 3-step approach (i.e., PFSS+SCS+1-DMK model) is much more reliable (e.g., stream interactions are taken into account) and permits direct comparison of predictions with observations.

RESULTS

A large number of test functions were tried using various combinations of the five photospheric/coronal parameters. The most interesting and/or promising were f_s, B_{ph}, and θ_b. The B_{ph} factor is especially interesting since flux tubes can have the same expansion factor but different values of B_{ph}. Do more intense magnetic flux tubes yield the same solar wind speed as WS would suggest? We were unable to find a velocity relationship dependent on B_{ph} (plus other parameters) that matched the observed wind speed at L1 any better than one of our best (though unpublished) empirical relationships

$$v_{sw}(f_s) = 285+650/(f_s)^{5/9} \text{ km s}^{-1}, \quad (1)$$

which is a function only of f_s.

Close inspection of the bottom panel of Figure 1 reveals the general pattern that the farther away an open field footpoint is from a coronal hole boundary (i.e., θ_b), the faster the corresponding solar wind speed. There are exceptions to this trend, but in most of those cases the tendency is for the expansion factors to be moderately large (e.g., just before the start of CR 1895 – many other case can be found). Note, that there is a broad data gap (with the values at the beginning and end of the gap connected by straight lines) between CR 1891 and 1892. The values there are not to be trusted. One will also note periods of rapid oscillation in θ_b (e.g., CR1897), we believe this primarily due to the coarseness of the grid used (5°×5°). The pattern described above and the clear correlation between v_{sw} and f_s, suggests using θ_b and f_s in combination to predict solar wind speed. We found that the function

$$v_{sw}(f_s,\theta_b) = 265 + \frac{25}{f_s^{2/7}}\left\{5 - 1.1e^{\left(1-\left(\theta_b/4\right)^2\right)}\right\}^2 \text{ km s}^{-1} \quad (2)$$

matched the solar wind speed observations at L1 rather well for the entire sequence of 15 Carrington rotations (CR1890-1904), which corresponds to the time interval from December 1994 to the end of 1995. (There were a number of large gaps in the photospheric field data in the early part of 1995 that appear to have degraded the results there.) For the entire 15 Carrington rotation sequence, the predictions obtained with the use of equation 2 agreed (qualitatively) with the WIND satellite observations generally better than those obtained using equation 1. CR 1896 is an especially nice example. For this particular rotation, Figure 2 shows a comparison of the solar wind speed predictions at L1, using both equations 1 and 2, with WIND satellite observations.

We were also interested in comparing model predictions with and without the SCS model's inclusion. We therefore re-ran the entire sequence of daily updated MWO maps using just the PFSS and 1-DMK model in combination with the later now transporting the solar wind from 2.5 $R_\odot$ to L1. Once again the solar wind speed predictions obtained using equation 2 show better overall agreement with observations than those obtained using equation 1 (see Figure 3). While

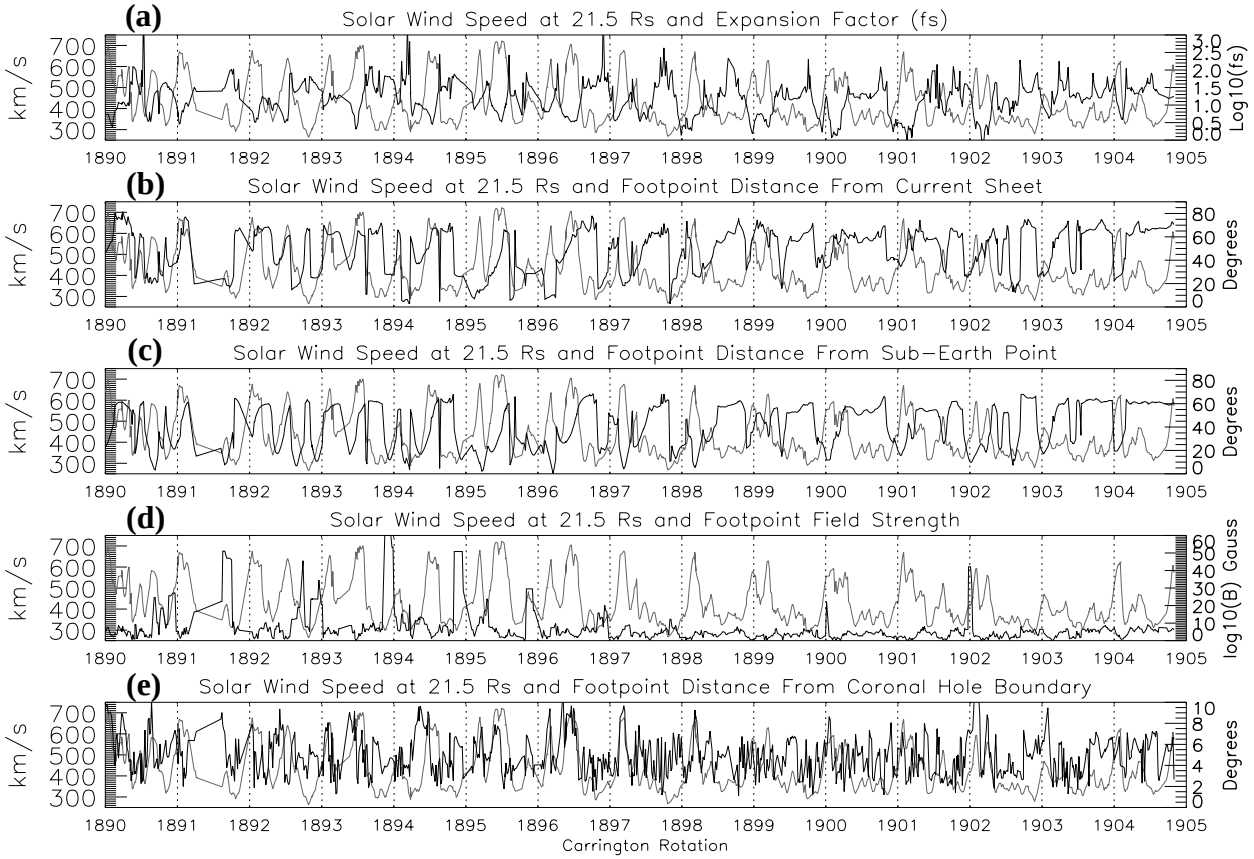

Figure 1. Five photospheric and coronal parameters (black lines) compared to solar wind speed (light gray lines). (**a)** Expansion factor (f_s), (**b)** footpoint distance from current sheet (θ_{cs}), (**c)** footpoint distance from sub-earth point (θ_{se}), (**d)** photospheric field strength (B_{ph}), and (**e)** footpoint distance from coronal hole boundary (θ_b).

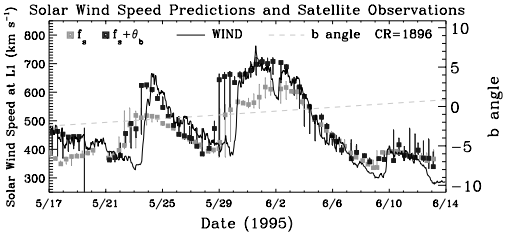

Figure 2. Comparison of solar wind speed observations (thin solid line) for CR 1896 with predictions using the PFSS+SCS+1-D kinematic model combination and equations 1 (black squares) and 2 (light gray squares). The vertical bars are uncertainty estimates determined by calculating the solar wind speeds for values located 2.5° above and below the sub-earth points.

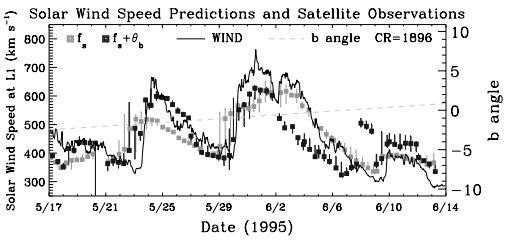

Figure 3. Same as Figure 2 expect now for the PFSS+1-D kinematic model combination.

equation 2 provides a clear improvement over equation 1, it is unclear whether the SCS model provides general improvement to the overall model prediction scheme. We find that when the solar wind source region (i.e., open field footpoints) is located at higher latitudes, the SCS+PFSS+1-DMK model combination produces results that typically agree better with observations than those made using the PFSS+1-DMK model combination. However, when the open field footpoints are located near the equator the reverse often appears to be true. The problem near the equator may be an artifact of the field line tracing routine used in the SCS model. It occasionally seems to get lost when the sub-earth point lies very close to the current sheet. Further investigation on this matter is required.

CR 1896 is a case where the inclusion of the SCS model improves model predictions at both high and low latitudes. Figure 4a shows the coronal holes as determined by the PFSS+SCS model combination, while Figure 5 shows them using just the PFSS model. The field polarity at the photosphere is indicated by the light (positive polarity) and dark (negative polarity) gray contours, while the light gray dots (the brighter the dot the smaller f_s and vice versa) identify the foot-

points of the open field lines (i.e., the coronal holes) at the photosphere. The white crosses near the equator mark the daily positions of the sub-earth point. The black straight lines identify the connectivity between the outer (open) boundary (i.e., 2.5 $R_\odot$ for the PFSS model or 21.5 $R_\odot$ for the PFSS+SCS model combination) and the source regions of the solar wind at the photosphere. For the large coronal hole located in the southern hemisphere (i.e., longitudes 176-236°), the PFSS+SCS model combination indicates that the solar wind (i.e., the stream observed at L1 beginning on May 30, 1995 in Figure 2 and 3) emerged from deeper within the hole than that implied by the PFSS model. The PFSS+SCS model also appears to explain better the properties of the stream (i.e., its short duration and the sharp velocity spike) that arrived 6 days before the larger one just mentioned (see Figure 2). The source regions of this stream cut directly across the equatorial hole, unlike the latitudinal meandering suggested by the PFSS model. Figure 4b is a plot of the field polarity at the outer boundary of the SCS model for CR 1896. In this figure, note that those portions of the sub-Earth track connected to the two coronal holes just discussed lie far from the current sheet. The field line tracing routine is more reliable in such cases, which helps explain why the PFSS+SCS model performed so well for CR1896.

SUMMARY

In addition to magnetic field expansion factor (f_s), solar wind speed also appears to be influenced by the minimum (spherical) angular distance (θ_b) that an open field footpoint lies from a coronal hole boundary. We have found a new empirical relationship for specifying solar wind speed near the Sun that is a function both of f_s and θ_b and which generally works much better (for the year 1995) than a relationship which is a function of f_s only. It is unclear whether the Schatten current sheet model produces a general improvement to the overall model prediction scheme. Our results suggest that it may (e.g., result from CR 1896), if the field line tracing routine used in it were improved. To establish the robustness of this new empirical relationship, we will test it for different periods of the solar cycle and perform a rigorous statistical analysis. We also plan to test the new empirical relationship using a 3D MHD solar wind model.

ACKNOWLEDGMENTS

We thank K. Ogilive, J. Steinberg, and A. Lazarus for allowing us access to the SWE key parameter data. We thank R. Ulrich for providing us access to daily updated MWO photospheric field synoptic maps. This work is supported by grants NSF ATM-0001851, ONR N00014-01-F-0026, and AFOSR/MURI.

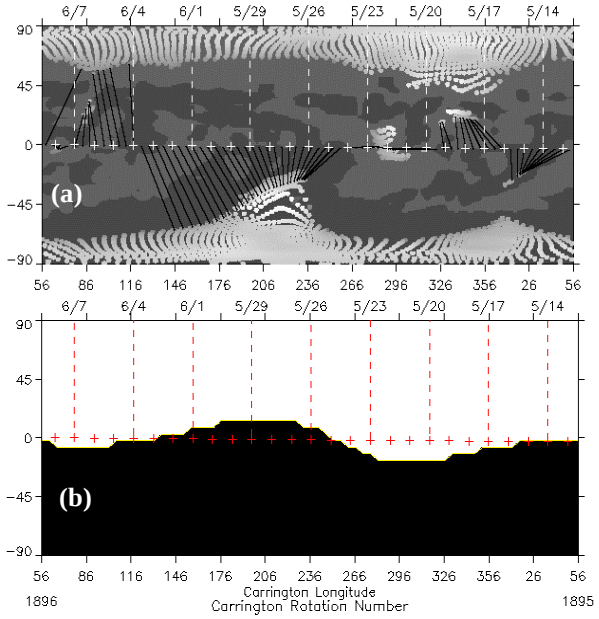

Figure 4. (a) Derived coronal holes for CR 1896 using the PFSS+SCS model combination. (**b**) IMF polarity at 21.5 $R_\odot$. Positive (negative) polarity is shaded white (black). See text for details.

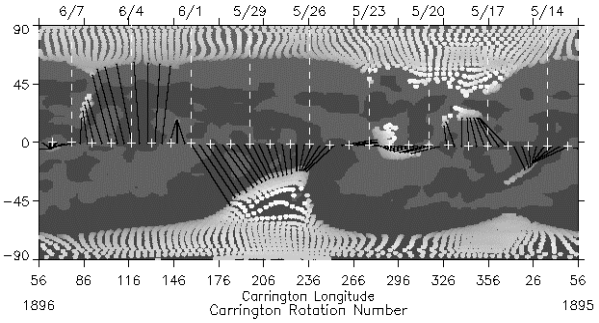

Figure 5. Same as Figure 4a except now using only the PFSS model.

REFERENCES

1. Hakamada, K., M. Kojima, Tokumaru, M., Ohmi, T., Yokobe, A., and Fujiki, K., *Sol. Phys.* in press (2002).
2. Wang, Y.-M., and Sheeley Jr., N. R., *Astrophys. J.* **355**, 726-732 (1990).
3. Schatten, K. H., Wilcox, J. M., and Ness, N. F., *Sol. Phys.* **9**, 442-455 (1969).
4. Altschuler, M. A., and Newkirk Jr., G., *Sol. Phys.* **9**, 131-149 (1969).
5. Wang, Y.-M., and Sheeley Jr., N. R., *Astrophys. J.* **392**, 310-319 (1992).
6. Arge, C. N., and Pizzo, V. J., *J. Geophys. Res.* **105**, 10,465-10,479 (2000).
7. Neugebauer, M., Liewer, P. C., Smith, E. J., Skoug, R. M., and Zurbuchen, T. H., *J. Geophys. Res.* in press (2002).
8. Schatten, K. H., *Cosmic Electrodyn.* **2**, 232-245 (1971).